Journal of Industrial and Engineering Chemistry xxx (xxxx) xxx

Contents lists available at ScienceDirect

Journal of Industrial and Engineering Chemistry

journal homepage: www.elsevier.com/locate/jiec

Highly mesoporous activated carbon fibers using high density polyethylene precursor with a multi-step stabilization technique for automobile carbon canister

Jeong-Rae Ahn [a,b], Hye-Min Lee [c,*], Byung-Joo Kim [a,d,*]

[a] Material Application Research Institute, Jeonju University, Jeonju 55069, Republic of Korea
[b] Department of Carbon Convergence and Composite Materials Engineering, Chonbuk National University, Jeonju 54896, Republic of Korea
[c] R&D Group 1, Korea Carbon Industry Promotion Agency (KCARBON), Jeonju 54853, Republic of Korea
[d] Department of Advanced Materials and Chemical Engineering, Jeonju University, Jeonju 55069, Republic of Korea

ARTICLE INFO

Article history:
Received 20 June 2023
Revised 5 August 2023
Accepted 14 August 2023
Available online xxxx

Keywords:
High-density polyethylene
Activated carbon fiber
Adsorption
Hydrocarbon emissions

ABSTRACT

In this study, activated carbon fibers (ACFs) for automobile carbon canisters were produced using high-density polyethylene (HDPE) fibers treated with a multistep stabilization process as the precursor. The stabilization of the HDPE fibers involved the following sequential steps: (1) electron beam irradiation, (2) mild sulfonation, and (3) dry oxidation. The stabilized fibers were carbonized at 900℃ in a nitrogen atmosphere. The carbonized fibers were activated at 900℃ in a water–vapor atmosphere from 30-60 min. The textural properties of the activated carbon fibers were determined using N_2/77 K adsorption–desorption isotherms. The specific surface area ranged from 1090 to 1980 m^2/g, and the total pore volume ranged from 0.56 to 1.11 cm^3/g. The specific surface area, micropore volume, and mesopore volume increased with increasing activation time. The fractions of micropores and mesopores were similar across all conditions, whereas the yield decreased gradually until 50 min, and then exhibited a sharp decline at 60 min. The butane working capacity increased as much as 56.24% as the increase in activation time. This can be attributed to the increase in butane activity owing to the increase in micropore volume, along with a decrease in butane resistivity caused by the increase in mesopore volume at a specific diameter.

Introduction

Automobile evaporative emissions occur from fuel tanks or engines when a vehicle is parked or idled and primarily consist of volatile organic compounds (VOCs) [1–4]. VOCs participate in atmospheric photochemical reactions, leading to the formation of ozone and particulate matter, some of which are known to be carcinogenic and fatal to human health [5–7]. A commonly adopted strategy to restrict evaporative emissions is to employ canisters filled with activated carbon (AC) to adsorb the evaporative emissions [8–10]. AC, known for its high chemical resistance and efficient removal of harmful substances, is widely used as a versatile adsorbent [11–13]. Furthermore, AC offers the advantage of cost-effective [14]. However, as concerns regarding environmental pollution have increased, regulations on evaporative emissions have become more stringent, resulting in an increasing demand for superior adsorbents [15].

Activated carbon fibers (ACF) have larger specific surface areas and total pore volumes than AC, with exposed micropores that facilitate faster adsorption kinetics [16–18]. However, the application of ACFs has been limited because of the high cost of their precursors. Therefore, active research is aimed at reducing the manufacturing cost of ACFs using low-cost precursors [19–22].

Polyethylene (PE) is an attractive precursor material for ACFs because of its lower cost and stable supply compared to other precursors such as polyacrylonitrile (PAN), pitch, and cellulose [19,20]. However, during carbonization, PE mostly decomposes into volatile aliphatic and olefinic compounds [23]. Therefore, to use PE as a precursor for ACFs, cross-linking is necessary to impart thermal stability.

Methods of cross-linking PE include ultraviolet radiation and dry oxidation [24]. In the case of ultraviolet radiation, pure PE is barely affected by UV, thus it needs to be mixed with other mate-

* Corresponding author at: Department of Advanced Materials and Chemical Engineering, Jeonju University, Jeonju 55069, Republic of Korea (B.-J KIM)
E-mail addresses: tm77kr@gmail.com (J.-R. Ahn), leehm@kcarbon.or.kr (H.-M. Lee), kimbyungjoo@jj.ac.kr (B.-J. Kim).

https://doi.org/10.1016/j.jiec.2023.08.024
1226-086X/

rials. Dry oxidation requires a temperature of 330 degrees, which is not suitable as it causes the shape of the PE fiber to collapse. There are also cross-linking methods using radiation, silane, peroxides, etc., but they are not suitable for PE fiber stabilization due to the limited penetration depth [24].

Previous studies have mainly used sulfonation for this purpose. In 2015, Kim et al. [25] used low-density polyethylene (LLDPE) as a precursor. They submerged LLDPE fibers in concentrated sulfuric acid, then heated it in the temperature range of 130-160℃ for a sulfonation duration of 60–240 min. Similarly, Wortberg et al. [26] selected HDPE fibers as the precursor in 2015. They soaked the HDPE fibers in concentrated sulfuric acid and conducted sulfonation at a temperature of 120℃ for up to 360 min. In 2020, Won et al. [27] manufactured a precursor by co-melting low-density polyethylene and HDPE. They performed sulfonation at temperatures ranging from 120-150℃ for a period of 60–150 min. It was noted that no hollows were formed in the carbonization stage when sulfonation was carried out for more than 120 min. In these studies, it was observed that the fibrous shape could be maintained after the carbonization process, provided that sulfonation was performed for a duration exceeding 120 min at temperatures higher than 120℃. In our previous studies, despite accelerating the reaction through the formation of radicals via electron beam irradiation, sulfonation still necessitates a duration of over 90 min and a temperature above 100℃ [28]. However, the concentrated sulfuric acid used in sulfonation is highly hygroscopic, resulting in decreased sulfonation efficiency as the exposure time in the atmosphere increases. Furthermore, as the duration of the sulfonation process increases, the potential for equipment corrosion could lead to rising process costs. Thus, reducing the sulfonation processing time is expected to improve the manufacturing process cost and process safety.

In this study, we applied a multistep stabilization technique that improved upon the electron-beam sulfonation process proposed in a previous study. To achieve a high crosslinking density while reducing the sulfonation processing time, we employed the electron-beam sulfonation-dry oxidation method to produce stabilized fibers. Furthermore, we prepared activated carbon fibers (ACFs) from stabilized fibers produced under various activation times and investigated their final textural properties and their correlation with the butane working capacity values [29].

Experimental

Materials

High-density polyethylene fibers (DURARON, Huvis, Republic of Korea) were used as precursors for ACFs synthesis. The fiber diameter was 15 μm, and sulfuric acid (H_2SO_4; 98 %, Daejung Chemical, Republic of Korea) was used as the crosslinking agent.

Preparation of stabilized fibers via multi-step stabilization method

The HDPE fibers were stabilized via irradiation with electron beams (1.5, 10 m/min, 1000 kGy). The primarily stabilized HDPE fibers were dipped in sulfuric acid (H_2SO_4, 98%, Daejung Chem., Siheung, Korea) and tension of 0.5 MPa was applied to prevent mechanical property reduction due to shrinkage (see Fig. 1). It was then heated to 100℃ at a rate of 1 ℃/min and sulfonated for 60 min. The sulfonated HDPE fibers were cooled to room temperature and rinsed with distilled water to remove the residual sulfuric acid. The rinsed fibers were dried in an oven at 100℃ for 12 h. After drying, fibers were heated in a SiC furnace with a horizontally mounted alumina tube (diameter 80 mm × length 1200 mm) at a heating rate of 5 ℃/min to 250℃ and then dry oxidized for

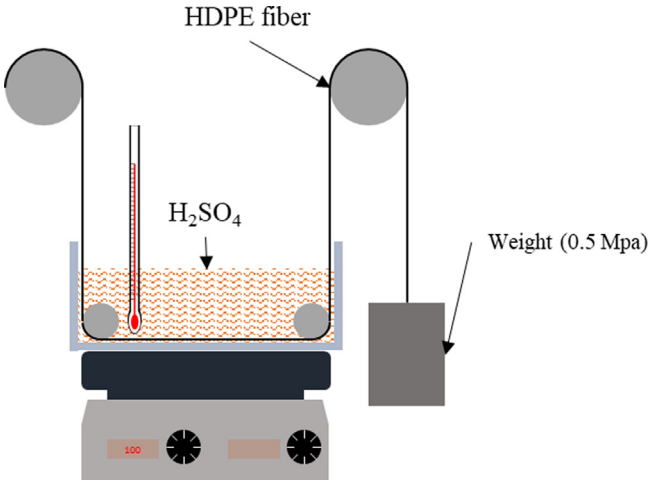

Fig. 1. Concept illustration of sulfonation instrument.

90 min under an air atmosphere (Air, 200 mL/min, 99.999%). The reaction mechanism of the Multi-step Stabilization Technique with HDPE is illustrated in Fig. 2.

Preparation of carbonized fibers and activated carbon fibers

The stabilized HDPE fibers were carbonized in a SiC furnace with a horizontally mounted alumina tube (diameter 90 mm × length 1000 mm) under a nitrogen atmosphere (N_2, 200 mL/min, 99.999%) by heating at a rate of 10 ℃/min to 900℃, followed by holding for 60 min. The carbonized HDPE fibers (CF) were activated in an iron-chromium-aluminum alloy furnace with a mounted stainless tube (SAE 310 s, diameter 80 mm × length 1200 mm) by heating at a rate of 10 ℃/min to 900℃ for 30–60 min under a water–vapor atmosphere (Distilled water, 0.5 mL/min), with an nitrogen atmosphere (N_2, 200 mL/min, 99.999%) maintained during the heating and cooling stages to control the effects of low-temperature activation. The prepared HDPE-based ACF were named using the following formats: PEACF-(Activation time). Table 1 lists the manufacturing conditions of the ACFs.

Morphology of carbonized fibers and activated carbon fibers

The cross-sectional morphologies of the prepared HDPE-based ACF were examined using scanning electron microscopy (SEM, AIS2000C, Seron Tech. Inc., Uiwang, Korea). To prevent deformation during cutting, the ACF were frozen in liquid nitrogen. The severed ACF were thawed to room temperature before being affixed to an SEM holder with carbon tape. The ACF were then coated with platinum nanoparticles (5 mA, 3 min) before measurement to prevent charge-up. The operating voltage of the SEM was 20 kV and the pressure of the analysis chamber was below 10^{-4} Pa.

Microstructure carbonized fibers and activated carbon fibers

The microstructure carbonized fibers and ACF were analyzed using X-ray Diffraction (XRD; MiniFlex, Rigaku, Tokyo, Japan). The XRD analysis was conducted at a rate of 4 °/min, over a range of 10 ∼ 70°, using CuKα radiation (1.5406 Å). The crystallite size, c-axis length (L_c), and a-axis length (L_a) were calculated from the XRD patterns using the Scherrer equation [30].

$$L = \frac{K\lambda}{B\cos\theta} \quad (1)$$

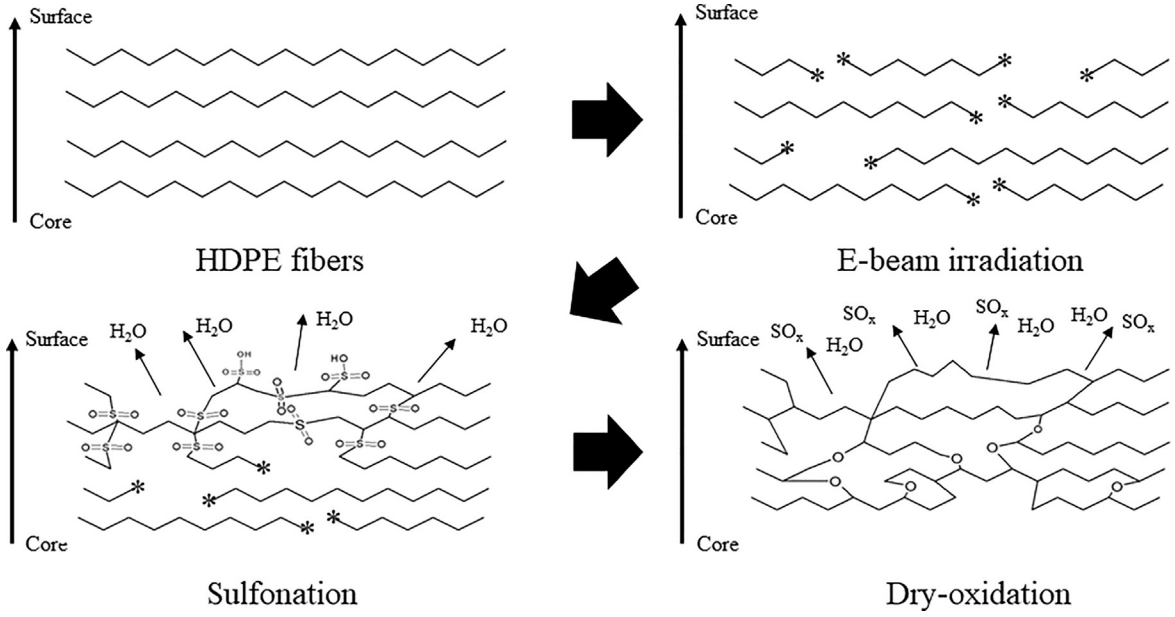

Fig. 2. Stabilization process of HDPE-based activated carbon fibers.

Table 1
Manufacturing Conditions and Sample Naming of HDPE-based Activated Carbon Fibers.

Sample name	E-beam	Sulfonation	Dry oxidation	Carbonization	Activation
PEACF-30	1000 kGy (1.5 MeV)	100℃, 60 min	250℃, 90 min	900℃, 60 min	900℃, 30 min (H_2O)
PEACF-40					900℃, 40 min (H_2O)
PEACF-50					900℃, 50 min (H_2O)
PEACF-60					900℃, 60 min (H_2O)

In Eq. (1), λ represents the wavelength of the X-rays used in the measurement and λ represents the Bragg angle. K is the shape factor (Lc = 0.9 and La = 1.84) and B is the full width at half maximum (FWHM).

Textural properties HDPE-based activated carbon fibers

The texture properties of ACF were analyzed using an isothermal gas adsorption analyzer (BELSORP-maxII, MicrotracBEL Corp., Osaka, Japan). All samples were loaded with 0.1 g into the measurement cell and then dried at 300℃ under a pressure less than 0.133 Pa for 12 h prior to the analysis. The specific surface area was calculated from the isotherm adsorption curve using the Brunauer-Emmett-Teller equation [31]. The micropore volume was calculated using the t-plot method [32], and the pore size distribution was analyzed using the non-localized density functional theory (NLDFT) [33].

Butane working capacity of HDPE-based activated carbon fibers

The butane working capacity (BWC) of the ACF were measured according to the ASTM-D5228 standard [29,34,35]. All samples were dried in a vacuum oven for more than 12 hours prior to the analysis, maintaining a temperature of 105℃ to prevent thermal degradation. The dried ACF (0.3 g) were loaded into a U-shaped measurement tube and then submerged in a constant-temperature water bath at 25℃. Nitrogen gas was flowed at a rate of 300 mL/min for 60 min to remove any impurities within the pores, such as residual carbon dioxide. The degassed ACF were subjected to a flow of n-butane at a rate of 250 mL/min for 15 min. Subsequently, the weight of the tubes was measured using a balance. Adsorption of n-butane was conducted for 10 min. This process was repeated until there was no further increase in mass attributable to the adsorption of n-butane. Once no further increase in mass due to n-butane adsorption was observed, nitrogen flowed through the ACF at a rate of 300 mL/min for 40 min to desorb the n-butane adsorbed onto the ACF. The change in weight of the measuring tube was determined using a balance. The difference in mass between the saturated and desorbed ACF was calculated and substituted into Eqs. (2)–(4) to determine the butane working capacity (BWC), butane activity (BA), and butane retentivity (BR).

$$\text{Butane working capacity}\,(\%) = \frac{(C-D)}{(B-A)} \times 100 \quad (2)$$

$$\text{Butane activity}\,(\%) = \frac{(C-D)}{(B-A)} \times 100 \quad (3)$$

$$\text{Butane retentivity}\,(\%) = \frac{(C-D)}{(B-A)} \times 100 \quad (4)$$

where A represents the weight of the measuring tube, and B is the weight of the measuring tube filled with the sample. C refers to the weight of the measuring tube filled with the sample after n-butane adsorption, and D indicates the weight of the measuring tube filled with the sample after desorption.

Results & discussion

Morphology of carbonized fibers and activated carbon fibers

The cross-sectional morphology of the ACF, as confirmed via SEM in Fig. 3, maintained the shape of the fibers even as the activation time increased. This suggests that the HDPE was cross-linked by dry oxidation. Additionally, hollows were identified in each fiber, and their diameters tended to increase with increasing activation time. The largest hollow, with a diameter of approximately 5 μm, is identified in Fig. 3 (e), where the activation time was 60 min. This phenomenon occurs because the cross-linking of the fiber during the stabilization process (including sulfonation and further dry oxidation) commences at the fiber surface, which is in direct contact with sulfuric acid and oxygen molecules and proceeds sequentially towards the core of the fiber. Hence, even after the carbonization process, the core of the fiber exhibits a lower level of crystallinity than the surface, and during activation, there is a greater mass loss in the fiber core than on the surface, which is perceived to contribute to the formation of hollows. Thus, it was inferred that the diameters of these hollows gradually increased as the activation time increased. The hollows initially resembled cracks, but gradually became circular as the activation time increased. This indicates that the difference in cross-linking density between the surface and core is the main mechanism of pore formation. In our previous report [28], HDPE fibers in which the sulfonation time did not exceed 90 min could develop circular hollows during the carbonization stage. However, in this study, hollow formation was not observed during the carbonization stage but was only observed during the activation stage in Fig. 3 (a). This observation indicates that the 60 min sulfonation treatment and subsequent dry oxidation are effective stabilization techniques.

Microstructure carbonized fibers and activated carbon fibers

Fig. 4 exhibits the XRD spectra of the HDPE-based ACF on the activation time. As shown in Fig. 4(a), which presents the full range of the XRD spectra, the position of the 002 peak is approximately 21.8°, which is different from the 26.56° position of the (002) peak in ideal graphite. The broad (10 *l*) peak observed at approximately 44.5° suggests that carbonized fibers (CF) and ACF are typically identified as isotropic carbons [36]. Furthermore, the absence of peaks associated with sulfur in the carbonized fibers suggests that the sulfonic groups formed in the HDPE molecular chains owing to sulfonation were completely removed after carbonization. The asymmetric shape of the 002 peak in the XRD spectra was evident and is known to originate from defects and turbostratic structures [37,38]. Also, the crystalline structure of carbonized fibers is generally known to improve above 1000℃ [39]. However, in the case of the CF produced in this study, the carbonization temperature was relatively low at 900℃, and due to the uneven cross-linking, it is considered that an amorphous structure and a turbostratic structure coexist [40]. Therefore, as shown in Fig. 4 (b), we deconvoluted the (002) peak into peaks around 20.87–20.96° and around 25.35–25.65°. The deconvoluted peak around 20.87–20.96° is presumed to contain a high amorphous content and tiny crystallites and was named less-developed crystalline carbon (LDCC) [38]. The peak around 25.35–25.65° was considered to mainly contain crystallites with a layered structure and was named more-developed crystalline carbon (MDCC)[38]. As the activation progresses, the half-widths of LDCC and MDCC decrease, presumably because oxidation predominantly occurs in the amorphous regions compared with the crystallite regions. The structural parameters calculated from the XRD patterns are listed in Table 2. In Table 2, comparing the L_c values of LDCC and MDCC in the carbonized fiber, LDCC is, on average, 13.20% larger than MDCC. Moreover, MDCC's d002 value is 21.48% lower than that of LDCC, with an average value of 3.48 Å. This is presumed to be a result of compression between the 002 planes due to an π bonding, which is more prominent in MDCC due to its higher degree of crystallinity.

The development of pores in ACF due to physical activation is known to be closely related to the crystallinity of the carbonized fibers and can be differentiated into three stages based on changes in the size of the microcrystals and the volume of micropores and

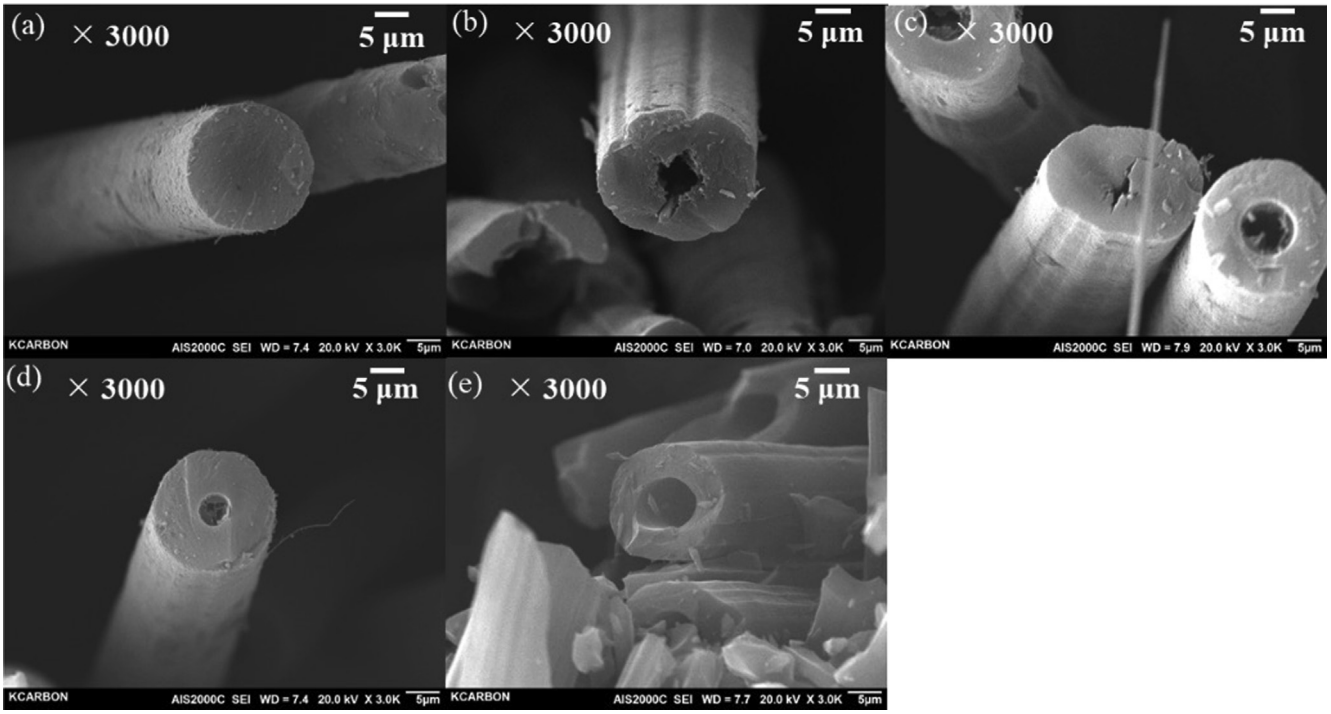

Fig. 3. Morphology of HDPE-based activated carbon fibers cross section as a function of activation time; (a) PECF, (b) PEACF-30, (c) PEACF-40, (d) PEACF-50, and (e) PEACF-60.

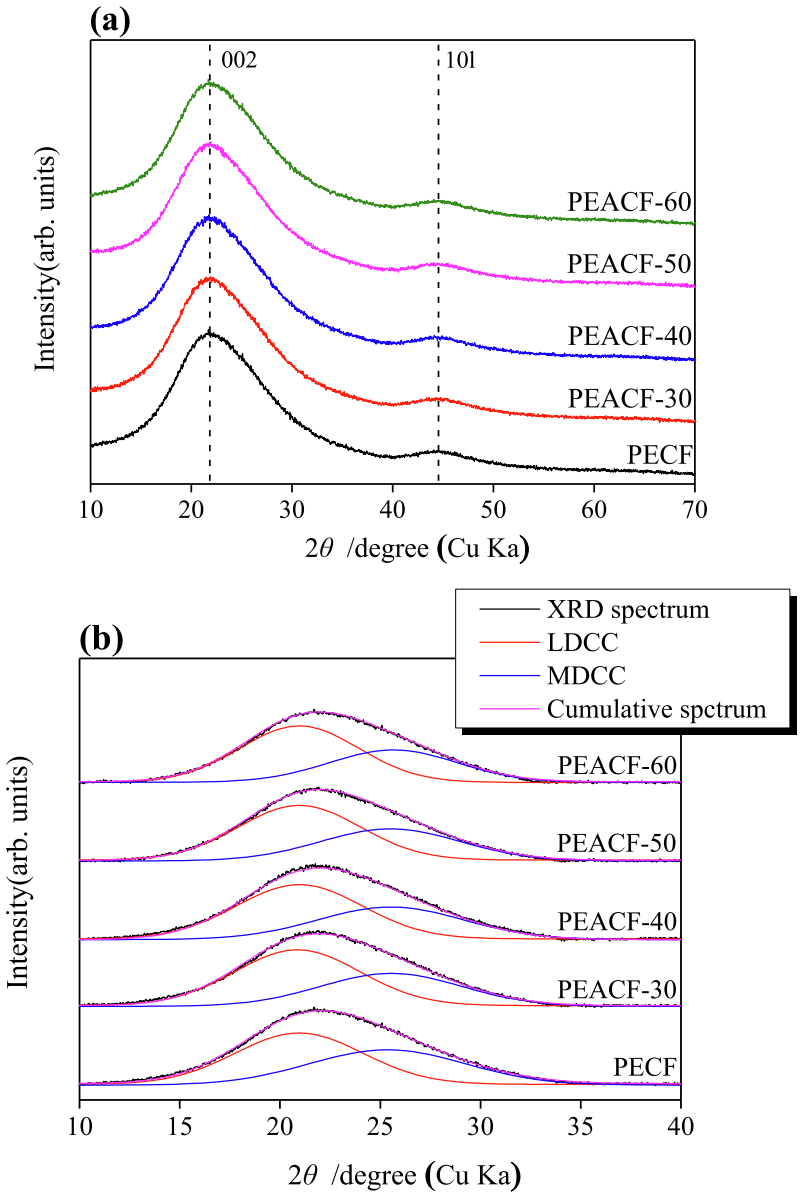

Fig. 4. X-ray diffraction Spectra of activated carbon fibers as a function of activation time; (a) full range and (b) $d_{(002)}$ range (LDCC: less-developed crystalline carbon and MDCC: more-developed crystalline carbon).

Table 2
Structural Parameters of HDPE-based Carbonized Fibers and Activated Carbon Fibers as a Function of Activation Time.

Sample name	**002**								**10 *l***		
	2θ		FWHM		d_{002}(Å)		L_c(Å)		2θ	FWHM	L_a(Å)
	LDCC	MDCC	LDCC	MDCC	LDCC	MDCC	LDCC	MDCC			
PECF	20.95	25.35	7.52	9.15	4.23	3.51	10.62	8.80	43.62	4.07	42.99
PEACF-30	20.87	25.54	7.38	8.29	4.25	3.48	10.83	9.72	43.69	3.98	43.98
PEACF-40	20.97	25.52	7.40	8.55	4.23	3.49	10.79	9.42	43.68	3.92	44.65
PEACF-50	20.97	25.51	7.15	8.20	4.23	3.49	11.18	9.82	43.68	3.85	45.46
PEACF-60	20.96	25.65	6.97	7.51	4.23	3.47	11.47	10.73	43.66	3.80	46.05

- **LDCC:** Less-developed crystalline carbon.
- **MDCC:** More-developed crystalline carbon.
- **FWHM:** Full width at half maximum.
- **L_c:** c-axis langth; **L_a:** a-axis langth.
- **PECF:** HDPE-based carbonized fibers.
- **PEACF:** HDPE-based activated carbon fiber.

mesopores [39]. Each of the three stages can be defined as follows: Stage 1 is characterized by the development of micropores owing to the predominant oxidation of amorphous areas, leading to an increase in L_c and L_a; Stage 2 involves the simultaneous oxidation of amorphous areas and the edges of crystallites due to continued activation, leading to the development of micropores and mesopores and an increase in L_c and L_a; Stage 3 is marked by a decrease in the volume of micropores and an increase in the volume of mesopores due to the oxidation of crystallite edges caused by the depletion of amorphous regions, leading to a decrease in L_c and L_a after the amorphous regions are depleted [40]. As shown in Table 2, as the activation time increased, the L_c and L_a values of the ACF increase by up to 21.93% and 7.11%, respectively. No decrease in crystallite size was observed as the activation time increased. This suggests that, as the activation process proceeds, oxidation occurs in the amorphous areas of the carbonized fibers. Until the activation time reached 60 min, the oxidation of the amorphous region was predominant compared with that of the crystallite region.

Textural properties HDPE-based activated carbon fibers

N_2/77 K isotherm adsorption–desorption curves are commonly used to analyze the pore characteristics of porous materials. Fig. 5 shows the N_2/77 K isotherm adsorption–desorption curves of the HDPE-based ACF. The isotherm adsorption curves of PEACF-30, PEACF-40, and PEACF-50 were classified as Type I(a) according to the IUPAC classification, indicating the presence of a porous structure with predominantly fine pores below 2 nm in diameter [41]. PEACF-60 is classified as Type I(b) and has a pore structure with larger micropores and an intermediate pore region (<2.5 nm) compared with the other samples [41]. The hysteresis loop shape is known to be related to specific pore characteristics, and the hysteresis loops observed in the synthesized ACFs were all classified as the H4-type according to the IUPAC classification. Therefore, it can be concluded that the synthesized ACFs possessed a pore structure characterized by slit-shaped pores [42].

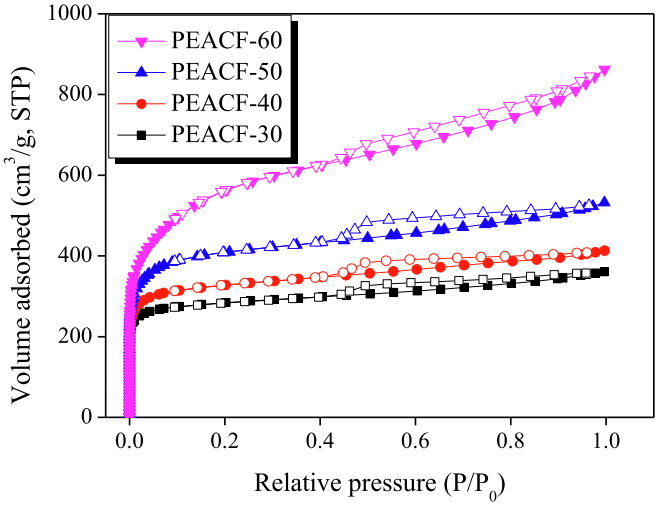

Fig. 5. N_2/77 K adsorption–desorption isotherm curves of activated carbon fibers as a function of activation time.

Table 3 presents the pore characteristics of the ACF calculated from the N_2/77 K isothermal adsorption–desorption curves. Both the specific surface area and total pore volume increased with increasing activation time; the specific surface area increased from 1090 m^2/g to 1980 m^2/g, and the total pore volume expanded from 0.56 cm^3/g to 1.11 cm^3/g. Furthermore, with an increase in activation time, the volumes of micropores and mesopores also increased, from 0.42 cm^3/g to 0.80 cm^3/g and from 0.14 cm^3/g to 0.31 cm^3/g respectively. During this process, the PEACF-40 sample showed a maximum micropore proportion of 76.56%. The mesopore volume of the PEACF-40 sample was initially 0.15 cm^3/g, but it increased from the PEACF-50 sample and reached 0.31 cm^3/g in the PEACF-60 sample, which represents a 106.67% increase compared to PEACF-40. These observations indicate that the activation phase up to 40 min can be characterized as the first stage of activation, as previously mentioned. Activation periods exceeding 50 min appear to correspond to the second stage of activation, characterized by the oxidation of amorphous and edges of crystallites. Moreover, the activation yield decreased from 66.18% to 21.82%. The most significant difference in the activation yield, a decrease of 27.95%, was observed between the 50–60 min interval. This phenomenon appears to be due to the oxidation of crystalline, which are denser than amorphous because of the oxidation at the edges of crystallites.

Fig. 6 shows the pore size distribution (PSD) of the HDPE-based ACF as determined using the NLDFT method. All samples primarily exhibited pore development within the micropore region, with the coexistence of pores having a narrow range of 0.45–0.75 nm and pores with a wider range of 0.65–2 nm. The PEACF-30 sample predominantly consisted of micropores with diameters ranging from 0.52 to 0.65 nm, however, in the PEACF-40, the distribution of micropores expanded to a range of 0.52 to 0.70 nm. Additionally, there was a noticeable increase in pores with diameters range 1–2 nm. The increase in pore volume of activated carbon by physical activation occurs in two ways: pore drilling (steady increase in pore diameter) and pore deepening (minimal change in pore diameter). As can be seen in Table 3, the total pore volume of HDPE-based ACF increased from 0.56 cm3/g to 1.11 cm3/g, with a significant increase in mesopore volume from the PEACF-50 as

Table 3
Textural Properties of HDPE-based Activated Carbon Fibers as a Function of Activation time.

Sample name	S_{BET} (m^2/g)	V_{total} (cm^3/g)	V_{micro} (cm^3/g)	V_{meso} (cm^3/g)	F_{micro} (%)	F_{meso} (%)	Yield (%)
PEACF-30	1090	0.56	0.42	0.14	75.00	25.00	66.18
PEACF-40	1250	0.64	0.49	0.15	76.56	23.44	56.42
PEACF-50	1560	0.82	0.60	0.22	73.17	26.83	49.77
PEACF-60	1980	1.11	0.80	0.31	72.07	27.93	21.82

S_{BET}: Specific surface area; BET method;. $\frac{p}{v(p_0-p)} = \frac{1}{v_m} + \frac{c-1}{v_m c} \cdot \frac{p}{p_0}$
V_{Total}: Total pore volume; BET method.
V_{micro}: Micropore volume; t-plot method.
V_{meso}: Mesopore volume; V_{Total}- V_{micro}.
Yield: (Weight of activated sample/Weight of carbonized sample input) × 100.

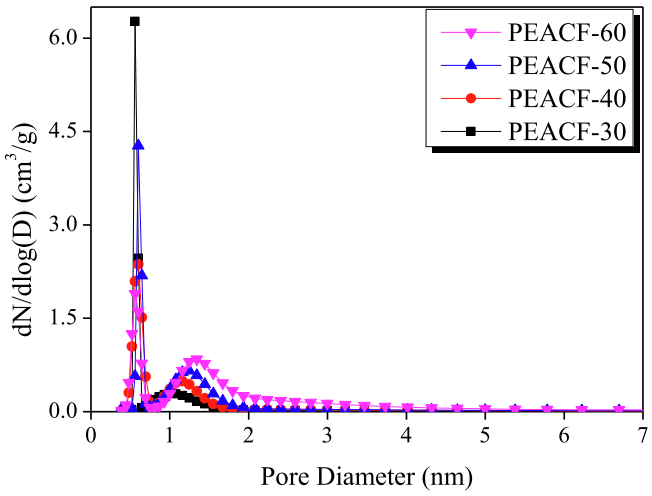

Fig. 6. Pore size distribution of the HDPE-based activated carbon fibers as a function of various activation time by the non-localized density functional theory (NLDFT) method.

the activation time increased. That is, up to the PEACF-30, pore development occurred due to pore deepening caused by the dominant oxidation in the amorphous region. In the PEACF-50 and PEACF-60, it is inferred that pore drilling occurred due to oxidation reactions at the edges of the crystallites and in the amorphous [43]. In other words, the change in the PSD of HDPE-based ACF was influenced by pore deepening in the initial stage of activation. However, as the activation time increased, the PSD curve was affected by pore drilling. Therefore, it is inferred that the pores with a diameter of 0.45–0.75 nm expanded and transitioned into pores with a diameter of 1–2 nm.

Butane working capacity of HDPE-based activated carbon fibers

The adsorption performance of the prepared ACF for fuel vapor was evaluated according to ASTM D5228. Fig. 7 shows the BWC, BA, and BR of the ACF as measured based on ASTM D5228. BA refers to the mass of n-butane adsorbed per unit mass of ACF, whereas BR represents the mass of n-butane remaining in the ACF per unit mass of ACF after desorption. BWC was obtained by subtracting BR from BA. As the activation time increased, BA rose

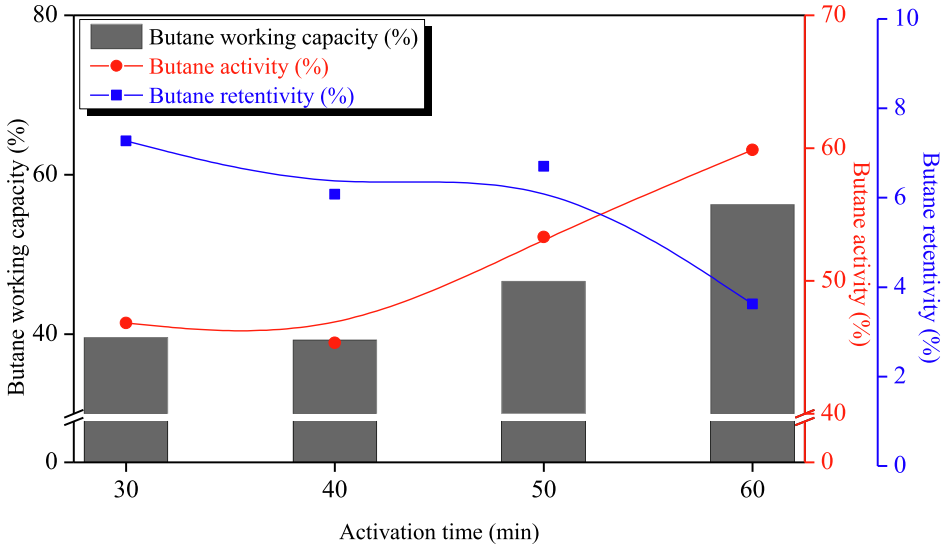

Fig. 7. Butane working capacity of HDPE-based activated carbon fibers as a function of activation time.

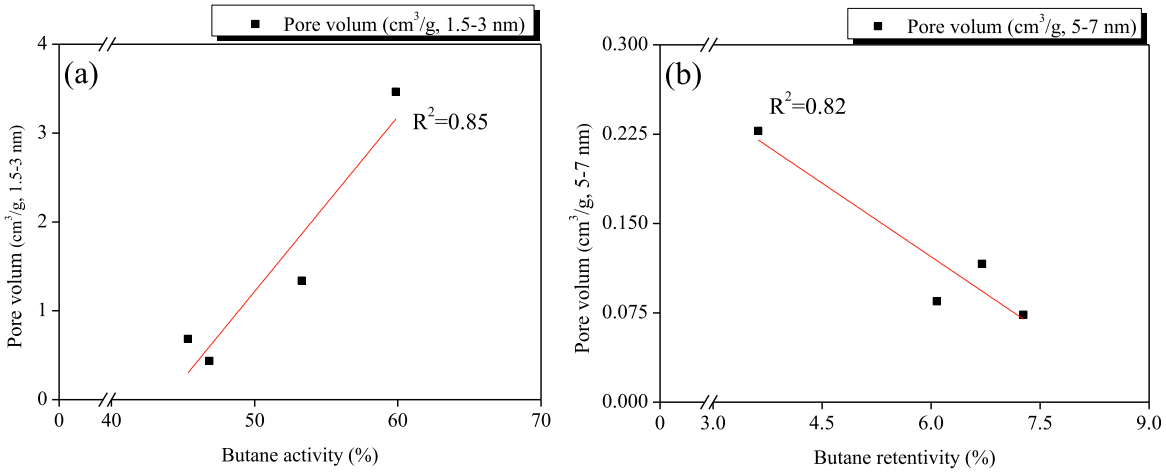

Fig. 8. Correlations between the butane activity with the pore volume (1.5–3.0 nm (a) and 5–7 nm (b)).

from 46.84% to 56.86%, whereas BR decreased from 7.27% to 3.62%. This suggests that the increase in the volumes of micropores and mesopores with increasing activation time could be the cause. BA and BR each have a correlation with the volume of micropores and mesopores, and notably, BA is known to be closely associated with pores of diameters in the range of 1.5–3.0 nm, while BR is closely associated with pores of diameters in the range of 5.0–7.0 nm [44].

Fig. 8 exhibits the correlation between the volumes of pores of diameters 1.5–3 nm and 5–7 nm in the HDPE-based ACF and BA and BR. As seen in Fig. 8 (a), the correlation coefficient (R^2) between BA and the volume of pores within the diameter range of 1.5–3.0 nm is 0.85, indicating a strong correlation. Similarly, Fig. 8(b) demonstrates that the correlation coefficient (R^2) between BR and the volume of pores within the diameter range of 5.0–7.0 nm is 0.82, also suggesting a strong correlation. As the activation time increased, the volume of pores in the HDPE-based ACF with diameters in the range of 1.5–3.0 nm increased from 0.05 cm^3/g to 0.16 cm^3/g, and the volume of pores with diameters in the range of 5.0–7.0 nm increased from 0.44 cm^3/g to 3.47 cm^3/g. The development of such sub-mesopores and mesopores is believed to result in an increase in BA and a decrease in BR, thereby enhancing BWC. According to previous our studies [35,44], adsorption predominantly occurs in micropores that are approximately 2–3 times larger than the molecular size of butane. The kinetic diameter of butane is 0.43 nm [45], and theoretically, effective adsorption should be observed in micropores larger than 1.2 nm. In this study, through pore size distribution analysis, a high tendency for BA was observed in the 1.5–3 nm range. This aligns well with the theoretical predictions. Meanwhile, BR is known to rely significantly on the volume of mesopores, as rapid desorption and facile diffusion of adsorbed molecules are essential [6,44]. In this study, we found a high correlation between BR and the volume of pores with diameters in the range of 5–7 nm. Therefore, it was observed that adsorbents with a pore structure that simultaneously satisfies high BA and low BR exhibit a larger BWC (BR-BA). In this study, the highest BWC was observed in samples that contained a substantial number of pores in both the 1.5–3 nm and 5–7 nm.

Conclusion

In this study, a multistep stabilization method incorporating electron-beam irradiation, sulfonation, and dry oxidation was applied to manufacture activated carbon fibers (ACF) for automobile carbon canisters using high-density polyethylene (HDPE) precursors. Despite the short sulfonation treatment time, all synthesized HDPE-based ACFs well maintained the fibrous form and demonstrated high activation yields of 49.77% at 1560 m^2/g and 21.82% at 1980 m^2/g, thereby confirming the effectiveness of the multistage stabilization method comprising electron beam irradiation, sulfonation, and air-thermal oxidation. The butane working capacity (BWC) and butane retention (BR) of all manufactured ACFs were found to be dependent on the volume of pores with diameters of 1.5–3 nm and 5.0–7.0 nm respectively. Among them, PEACF-60 exhibited the highest BWC value, as much as 56.24%.

Declaration of Competing Interest

The authors declare that they have no known competing financial interests or personal relationships that could have appeared to influence the work reported in this paper.

Acknowledgement

This research was supported by the Nano-Material Technology Development Program through the National Research Foundation of Korea (NRF) funded by the Ministry of Science and ICT (NRF-2019M3A7B9071501) and the Ministry of Trade, Industry, and Energy Technology as Innovation Program (Project No. 20013038).

References

[1] C.B. Almquist, J. Kocher, K. Saxton, L. Simonson, A. Danciutiu, P.J. Nguyen, J. Bain Catalysts 1 (3) (2022) 85.
[2] L. Romagnuolo, R. Yang, E. Frosina, G. Rizzoni, A. Andreozzi, A. Senatore, Renew. Sustain. Energy Rev. 116 (2019).
[3] P. Dai, Y. Ge, Y. Lin, S. Su, B. Liang, Fuel 113 (2013) 10–16.
[4] S. Inomata, H. Yamada, H. Tanimoto, Curr. Pollut. Rep. 2 (2016) 188–199.
[5] H. Liu, H. Man, M. Tschantz, Y. Wu, K. He, J. Hao, Environ. Sci. Tech. 49 (2015) 14424–14431.
[6] X. Li, L. Zhang, Z. Yang, P. Wang, Y. Yan, J. Ran, Sep. Purif. Technol. 235 (2020).
[7] K. Isinkaralar, A. Turkyilmaz, Carbon Lett. 32 (2022) 1781–1789.
[8] L. Romagnuolo, E. Frosina, A. Andreozzi, A. Senatore, F. Fortunato, Fuel 304 (2021).
[9] L. Romagnuolo, E. Frosina, F. Fortunato, A. Andreozzi, A. Senatore, Appl. Therm. Eng. 209 (2022).
[10] H. Yamada, The Science of the Total Environment 449 (2013) 143–149.
[11] Z. Zhang, T. Wang, H. Zhang, Y. Liu, B. Xing, The Science of the Total Environment 757 (2021).
[12] V. Nejadshafiee, M.R. Islami, Mater. Sci. Eng. C 101 (2019) 42–52.
[13] L. Niazi, A. Lashanizadegan, H. Sharififard, J. Clean. Prod. 185 (2018) 554–561.
[14] C. Lim, C.H. Kwak, S.G. Jeong, D. Kim, Y.-S. Lee, Carbon Lett. 33 (2022) 139–145.
[15] H.-M. Lee, J. Baek, K.-H. An, S.-J. Park, Y.-K. Park, B.-J. Kim, Ind. Eng. Chem. 58 (2018) 736–741.
[16] R. Awad, A. Haghighat Mamaghani, Y. Boluk, Z. Hashisho, J. Chem. Eng. 410 (2021).
[17] J. Chen, J. Xie, C.Q. Jia, C. Song, J. Hu, H. Li, J. Chem. Eng. 450 (2022).
[18] Y.-H. Wang, S. Bayatpour, X. Qian, B. Frigo-Vaz, P. Wang, Colloids Surf. APhysicochem. Eng. Asp. 612 (2021).
[19] Q. Wang, W. Ma, E. Yin, S. Yu, S. Wang, H. Xiang, D. Li, M. Zhu, ACS Appl. 3 (2020) 9360–9368.
[20] K.-W. Kim, H.-M. Lee, S.-H. Kang, B.-J. Kim, Polymers 13 (2021) 3918.
[21] H. Wang, J. Yang, J. Li, K. Shi, X. Li, SN Appl. Sci. 1 (2019).
[22] S.-H. Kang, H.-M. Lee, K.-W. Kim, B.-J. Kim, J. Ind. Eng. Chem. 121 (2023) 401–408.
[23] E. Frank, E. Muks, A. Ota, T. Herrmann, M. Hunger, M.R. Buchmeiser, Macromol. Mater. Eng. 306 (2021).
[24] T. Röding, J. Langer, T. Modenesi Barbosa, M. Bouhrara, T. Gries, Appl. Res. 1 (2022).
[25] J.W. Kim, J.S. Lee, Carbon 94 (2015) 524–530.
[26] G. Wortberg, A. De Palmenaer, M. Beckers, G. Seide, T. Gries, Fibers 3 (2015) 373–379.
[27] J.S. Won, H.R. Lee, M.J. Lee, M.H. Jeon, S.G. Lee, Y.L. Joo, Polymers 12 (2020) 2895.
[28] S.-H. Kang, K.-W. Kim, B.-J. Kim, Polymers 13 (2021) 2157.
[29] American Society for, Testing and Materials. Standard Test Method for Determination of Butane Working Capacity of Activated Carbon; ASTM Standard D5228-16, ASTM, West Conshohocken, PA, USA, 1992.
[30] J. Biscoe, B.E. Warren, J. Appl. Phys. 13 (1942) 364–371.
[31] S. Brunauer, P.H. Emmett, E. Teller, J. Am. Chem. Soc. 60 (1938) 309–319.
[32] A. Galarneau, F. Villemot, J. Rodriguez, F. Fajula, B. Coasne, Langmuir 30 (2014) 13266–13274.
[33] C. Lastoskie, K.E. Gubbins, N. Quirke, The Journal of Physical Chemistry 97 (1993) 4786–4796.
[34] J.-Y. Lee, H.-M. Lee, B.-J. Kim, Carbon Lett. (2023).
[35] H.-M. Lee, B.-H. Lee, K.-H. An, S.-J. Park, B.-J. Kim, Carbon Lett. 30 (2019) 297–305.
[36] J.-H. Bang, B.-H. Lee, Y.-C. Choi, H.-M. Lee, B.-J. Kim, Int. J. Mol. Sci. 23 (2022) 853.
[37] S. Zhang, Q. Liu, H. Zhang, R. Ma, K. Li, Y. Wu, B.J. Teppen, Carbon 157 (2020) 714–723.
[38] S.-M. Lee, S.-H. Lee, J.-S. Roh, Crystals 11 (2021) 153.
[39] P. Gutmann, J. Moosburger-Will, S. Kurt, Y. Xu, S. Horn, Polym. Degrad. Stab. 163 (2019) 174–184.
[40] J.-S. Jeong, K.-W. Kim, D.C. Chung, K.-H. An, B.-J. Kim, Carbon Lett. 32 (2021) 567–579.
[41] J.-H. Kim, S.-C. Jung, H.-M. Lee, B.-J. Kim, Int. J. Mol. Sci. 23 (2022) 3680.
[42] M. Thommes, K. Kaneko, A.V. Neimark, J.P. Olivier, F. Rodriguez-Reinoso, J. Rouquerol, K.S.W. Sing, Pure Appl. Chem. 87 (2015) 1051–1069.
[43] J.-H. Kim, Y.-J. Kim, S.-C. Kang, H.-M. Lee, B.-J. Kim, Minerals 13 (2023) 802.
[44] B.-H. Lee, H.-M. Lee, D.C. Chung, B.-J. Kim, Nanomater. 11 (2021) 673.
[45] Y. Hasegawa, T. Nagase, Y. Kiyozumi, F. Mizukami, J. Membr. Sci. 294 (2007) 186–195.